

SPE 64998

Setting Rheological Targets for Chemical Solutions in Mud Removal and Cement Slurry Design

I.A. Frigaard, SPE, University of British Columbia, and M. Allouche, SPE, Schlumberger, and C. Gabard-Cuoq, SPE, Université Pierre et Marie Curie & Schlumberger

Copyright 2001, Society of Petroleum Engineers Inc.

This paper was prepared for presentation at the 2001 SPE International Symposium on Oilfield Chemistry held in Houston, Texas, 13–16 February 2001.

This paper was selected for presentation by an SPE Program Committee following review of information contained in an abstract submitted by the author(s). Contents of the paper, as presented, have not been reviewed by the Society of Petroleum Engineers and are subject to correction by the author(s). The material, as presented, does not necessarily reflect any position of the Society of Petroleum Engineers, its officers, or members. Papers presented at SPE meetings are subject to publication review by Editorial Committees of the Society of Petroleum Engineers. Electronic reproduction, distribution, or storage of any part of this paper for commercial purposes without the written consent of the Society of Petroleum Engineers is prohibited. Permission to reproduce in print is restricted to an abstract of not more than 300 words; illustrations may not be copied. The abstract must contain conspicuous acknowledgment of where and by whom the paper was presented. Write Librarian, SPE, P.O. Box 833836, Richardson, TX 75083-3836, U.S.A., fax 01-972-952-9435.

Abstract

A major application area for chemistry-based solutions in oilfield cementing is in the reliable design of fluid rheologies for different purposes. A common situation is that one visco-plastic fluid will be displaced by another fluid along some sort of channel, e.g. a pore-space or the annulus during cementing. Whether the resident fluid is completely displaced will depend largely upon the fluid rheologies and hence on the chemical design of the fluids. Understanding the mechanics of this process enables one to set rheological targets for applied chemistry solutions.

We present new results of university and industrial research into the displacement of visco-plastic fluids along long ducts, (pipes and slots). The research combines laboratory experiments with computational studies and with detailed mathematical analysis of the fluid mechanics. The results are both new and surprising, being in many respects counter to accepted oilfield intuition.

The direct application of these results is in the design of spacer and cement slurry properties for effective mud removal during primary cementing. The breakdown of zonal isolation can sometimes be attributed to poor bonding of the cement to the casing and formation, due to the existence of residual mud layers on the walls of the annulus after cementing, i.e. the formation of a so-called "*wet micro-annulus*". It is possible to detect such layers using advanced ultrasonic cement evaluation logs.

A visco-plastic fluid displaced by a fluid with a smaller yield point can leave a static residual layer of gelled fluid on the walls of the channel. We show that it is possible to predict the

maximum static layer that can remain. Actual static layers that are observed in simulations and experiments are much thinner than the maximum layer. Additionally, the variation in static layer thickness with rheological and process parameters is not at all intuitive. For example, increasing the mean velocity can actually increase the static layer thickness and increasing the yield stress of the fluid to be displaced can result in a thinner static layer! These results are confirmed by laboratory experiments, computational simulation and mathematical analysis.

The results are quite novel. Displacements with viscous fluids do not leave fully static residual wall layers, unless other physico-chemical phenomena are present. Similarly, previous oilfield investigators have considered that, in order to remove a layer, it is necessary to design the fluid rheology so that the maximum static layer predicted has zero thickness. We argue that this is rarely necessary, although sufficient, and that static wall layers can be removed with reduced rheologies.

The most significant aspect of this research is that finally, with knowledge of local displacement velocities and fluid properties, we are able to predict the likely risk of a wet micro-annulus occurring during a primary cementing operation. Conversely, we are able to make recommendations for rheological fluid properties that are sufficient to avoid a wet micro-annulus and thus to enhance the prospect of complete zonal isolation during primary cementing. This sets the targets for applied chemistry solutions.

Introduction

A key application for chemistry-based solutions in oilfield cementing is the design of fluid rheologies for laminar displacements of mud in the annulus. This topic has been the subject of study for many years, since the seminal work in Ref. 1. Although there exists widespread agreement in the industry that displacements in the turbulent flow regime produce better-cemented wellbores, fully turbulent cementing displacements are often not possible. Either well security restrictions prevent this, or only part of a fluid sequence will be turbulent, i.e. the wash, or turbulence will be achieved only on the wide side of the annulus. Therefore, laminar cementing displacement flows retain significant process interest and will continue to do so for the foreseeable future, particularly in

difficult wells where frictional pressure restrictions are most severe.

Incomplete mud removal can manifest in different ways. First, a coherent mud channel can form on the narrow side of the eccentric annulus. Second, residual mud or spacer can contaminate the cement as it sets. Third, mud may remain static in layers stuck to the inner and outer walls of the annulus. In the first or last case, the residual mud dehydrates as the cement sets and allows a porous conduit to develop in the annulus. In the case of severe contamination, the cement may not properly set. This paper focuses on predictive methods for the third case, namely having layers of residual mud left on the walls of the annulus during displacement, a so-called fluid-filled micro-annulus.

Two major problems result from the existence of mud channels and micro-annuli in finished wellbores. First, well production can be severely compromised by poor zonal isolation. Second, surface casing vent flows can develop throughout the lifetime of the well, making environmentally safe abandonment impossible, without expensive remedial treatment. While the former is the traditional motivation for primary cementing, it is the latter problem that is becoming increasingly important to the industry, and increasingly visible, as evidenced by the large numbers of temporarily shut-in and/or suspended wells that exist worldwide.

Design methodologies for primary cementing that consider the rheology of the fluids have a long history. The possibility of a mud channel forming on the narrow side of the annulus was identified in Ref. 1. The reasoning used in Ref. 1 is essentially a hydraulic approach. Extensions have led to systems of design rules for laminar displacements, (Refs. 2-6), based on hydraulic reasoning. In general, these rule sets state that the flow rate must be sufficiently high to avoid a mud channel on the narrow side of the annulus, that there should be a hierarchy of the fluid rheologies and fluid densities. Successful applications of such rule-based systems are given in Refs. 7-9. Although such approaches obviously contain a number of physical truths, the level of fundamental understanding is low and we can expect a reasonably high degree of conservatism in predictions made. A further problem with such systems is in making predictions for highly deviated and horizontal wellbores, since positive density differences, which help displacements in near-vertical wells, tend to cause slumping towards the lower side of the annulus in highly deviated sections, (Refs. 10-12). In such wellbores, the focus must clearly be on rheology design.

More fundamental work has focused on computing the entire annular flow. However, this work is relatively recent. The first reliable analyses of narrow eccentric annular flows of visco-plastic fluids were conducted in the early 1990's, (Refs. 13,14), and these only for flows of a single fluid and in two dimensions. Three-dimensional Newtonian displacements in eccentric annular geometries have been computed in Refs. 15 and 16, but a fully three-dimensional approach is restrictive in designing displacements over the scale of the wellbore. A different approach averages across the narrow annular gap and solves the resulting two-dimensional model, (Refs. 17-19).

This approach effectively models the annulus as an enormous eccentric annular Hele-Shaw cell. There is undoubtedly validity to this approach, due to the hierarchy of length-scales present in primary cementing geometries (i.e. axial length \gg circumference \gg annular gap). Indeed, in cases where the displacement of mud across the annular gap is complete, the approach in Refs 18 and 19 appears to be a rational way to model primary cementing displacements for design applications, and it is underexploited.

In this paper, we consider what happens when the displacement of mud across the gap is not complete and layers of mud remain behind on the walls of the annular gap. Such an approach has been considered, in very simplified form, in Refs. 20,21. Apart from Refs. 20-21, the phenomenon of static residual layers of a visco-plastic fluid being left on the walls of a channel during displacements (by a gas) has been studied in Ref. 22. Extensions and refinement of the analyses in Refs. 20 and 21 has led to the concept of erodability of mud layers, (Ref. 23). In this model, it is deemed necessary for the shear stress generated at the wall during a displacement to exceed the strength (modelled as a yield stress) of mud left on walls, in order for the mud to be removed from the wall. The results that we present later show that this is not in general necessary, although it is a sufficient condition.

Methodology

Cementing displacement flows are extraordinarily complex because of three factors: the complex rheologies of the fluids; the eccentric annular geometry; the interaction between fluids. Geometrically however, the annular gap width is narrow relative to the circumferential and axial length-scales. This prompts us to reduce the geometrical complexity by considering first a long slot. Apart from this simplification, we retain the full complexity of the problem and build our understanding through a combination of mathematical analysis, computational fluid dynamics (CFD) simulations and small-scale fluid flow experiments.

Mathematical Model

As stated above, our modelling is focused on a slot geometry, which represents a longitudinal section of a narrow annulus (Fig. 1). The phenomenon that we study is that of a layer of drilling mud remaining static and stuck to the wall of a slot as the displacing fluid passes. This ability of a fluid layer to remain fully static at the wall is a result of the plasticity of the fluid. To accommodate this phenomenon at the simplest level, we assume that our fluids are represented as Bingham fluids. A second assumption is to consider water-based fluids, where surface tension effects are not important. Since this paper focuses on rheology effects, we also assume that the fluid densities are matched.

We consider a slot of width $2D$ initially full of drilling mud, with yield point YP_m and plastic viscosity PV_m . The mud is flowing at a mean velocity U_0 . We displace the mud with a spacer (or slurry) that has yield point YP_s and plastic viscosity PV_s , keeping the mean velocity at U_0 . Our

situation is modelled by the two-dimensional Navier-Stokes equations, valid in each fluid region, and by assuming the continuity of stress and velocity at the interface between the two fluids.

When we scale the Navier-Stokes equations, under the above assumptions, only four dimensionless parameters remain. Using the principle of dynamic similarity, these four parameters will govern all features of the flow, including the phenomena of static wall layers. These four parameters are the two dimensionless yield stresses $\tau_{Y,m}$ and $\tau_{Y,s}$,

$$\tau_{Y,m} = \frac{YP_m}{\rho U_0^2} \quad \tau_{Y,s} = \frac{YP_s}{\rho U_0^2}, \quad (1)$$

and the two dimensionless plastic viscosities μ_m and μ_s ,

$$\mu_m = \frac{PV_m}{\rho DU_0} \quad \mu_s = \frac{PV_s}{\rho DU_0}. \quad (2)$$

Here ρ is the fluid density. Our analysis uses this dimensionless model and the later results are presented in terms of combinations of these four parameters.

CFD Simulations

Apart from a mathematical analysis of the displacement flow, we have also conducted a large number of simulations of the displacement, for different rheological parameters. The simulations actually solve the fully transient 2D Navier-Stokes equations, for the described displacement. The computations are carried out using the CFD code FIDAP, version 8.0. This is a finite element based code. The two fluids are handled by FIDAP using the volume of fluid (VOF) method.

Each simulation constitutes a numerical experiment in which we attempt to displace the mud from a long slot of aspect ratio 30:1. The flow is assumed symmetric about the slot center-line and only a half-slot is used for the computations. We pump in the displacing fluid at constant flow rate until one slot volume has been pumped. We then measure the average thickness of mud layer that is left on the wall. The numerical experiment is repeated for a range of different fluid rheologies and the results are used to compare against our mathematical analysis.

Experimental Apparatus

The third very important component of our methodology is the use of small-scale experiments. Unfortunately, it is not really feasible to use a slot for experimental displacements. To do so would require an apparatus where two flat plates are separated by a small gap, i.e. a non-capillary scale Hele-Shaw cell. For such experiments there are difficulties in ensuring that the flow remains uniform in the depth direction. As shown in Refs. 24 and 25, such flows often become unstable in the depth direction. This is the classical instability of Saffman and Taylor (Ref. 26).

To avoid these difficulties, our experiments are based on a pipe. As with the slot, stable laminar pipe displacements are symmetric and the base flow is a Poiseuille shear flow. We are

able to generalize our mathematical results to this geometry and also to run simulations. In this way we can make comparisons against the equivalent theoretical and numerical predictions.

The experimental apparatus consists of a long tube of 24mm in diameter. The tube is initially filled with an aqueous Carbopol solution, and this is displaced using either water or Carbopol solutions of the same density but of lower yield stress. Carbopol solutions are largely inelastic but have a yield stress that can be controlled by varying the concentration. The pipe is housed in a large-volume aquarium/bath in which the temperature is controlled. Flow rates are carefully regulated to give mean velocities in the range 0.001 to 0.2m/s. A schematic of the experimental set-up is shown in Fig. 2. Three measurement techniques are used to measure the displacement. First, a global measurement of concentration of the fluids exiting the pipe is made using conductivity. Second, video visualization of the displacement is made. Third, acoustic transducers are positioned at different heights along the pipe. The speed of sound is different in the two fluids and this method allows pointwise measurement of layer thickness. Although requiring some expertise to implement, the typical precision of the acoustic method less than 2.5% of the pipe radius. Combined with the video, the measurement of the displacement is quite complete. The experimental apparatus is described in detail in Ref. 27.

Mathematical Analysis and Results

Here we give an overview of the mathematical results that can be derived for this problem. The actual derivation is in places difficult and is described fully in Refs. 28 and 29.

Maximum Layers

The simplest analysis that we have conducted concerns the prediction of a maximum static layer thickness of mud that can remain on the walls of the slot. For this we consider the scenario in Fig. 3, where the displacement front has long passed a point in the slot, leaving behind a parallel static layer of mud on the wall. Since the mud is static, the entire flow must pass through the spacer layer. For a vanishingly thin mud layer, the spacer flow would be identical with that for the spacer passing alone through the slot. If the shear stress generated at the wall in this flow exceeds the yield stress of the mud, it would not be possible to have an infinitesimally thin layer of mud left at the wall. Therefore, a necessary condition for a mud layer to remain static at the wall is:

$$YP_m > [\text{WALL SHEAR STRESS}]. \quad (3)$$

Since the wall shear stress in the spacer must exceed the yield stress of the spacer, a sufficient condition to avoid having a mud layer on the wall that is static, is to ensure that:

$$YP_s > YP_m. \quad (4)$$

If we have a finite thickness of static mud layer, Equation 3 still remains valid. For a finite static thickness, all of the flow passes through the spacer layer. We can compute the shear stress in the spacer layer, assuming the mud to be static, and

continue the shear stress through the static mud layer. If the wall stress is less than the yield stress of the mud, the layer is indeed static (Fig. 4) otherwise, it moves.

Consider now a progressively thick static mud layer in a channel. In keeping the mean velocity fixed and the mud layer static, we are forcing the same flow rate of fluid through a progressively thinner spacer channel. As the channel becomes smaller, the stress at the interface increases and therefore also the stress at the wall. For an infinitesimally thin spacer channel in the center of the slot, it would require an infinite interfacial stress to pass a finite flow rate through the channel. Therefore, eventually, we know that the stress at the wall will exceed YP_m for a sufficiently large layer thickness.

This argument is wholly physical, but the same argument can be formulated rigorously in mathematical terms. We denote the mud layer thickness in this flow by Dh , i.e. h is the fraction of the slot that contains mud. The physical argument says that there will be a maximum fraction, say h_{\max} , such that mud layers with thickness less than Dh_{\max} will be static and those greater than Dh_{\max} will be mobile. The full mathematical analysis is in Ref. 28. It can be shown that h_{\max} depends on only two dimensionless parameters. First is the Bingham number of the spacer, B_s , and second is the ratio of the two yield points, ϕ_Y .

$$B_s = \frac{D \times YP_s}{U_0 \times PV_s}, \quad \phi_Y = \frac{YP_s}{YP_m} \quad (5)$$

Fig. 5 plots contours of the maximum layer thickness h_{\max} against these two parameters. The shaded area denotes the limit where the shear stress at the wall exceeds the yield stress of the mud, which shows that the condition in Equation 4 is sufficient, but not necessary.

Minimum Layers

In observing both small-scale experimental displacements and the results of CFD simulations, it was noted that the displacing fluid moved steadily along the center of the duct in an apparently stable finger shape, leaving behind uniform static layers of fluid. The above analysis, for h_{\max} , is relevant to the flow in the parallel layers behind the propagating finger. A more complex analysis focuses on the propagating finger displacement flow itself (Ref. 29).

Consider a frame of reference that moves with the steady speed of the displacing finger. In this frame of reference, the interface between the two fluids remains stationary. Upstream and downstream from the interface, in the far-field, the fluid velocities are again parallel. The downstream velocity profile will be a classical Bingham-Poiseuille profile in the mud and the upstream velocity profile will be a multi-layer flow, with the wall layers stationary and the central spacer layer having a Bingham-Poiseuille profile, as shown schematically in Fig. 4.

Consider now the situation where the static mud layer is vanishingly thin and the upstream flow consists solely of the spacer. The same flow rate of mud and spacer passes through the slot, but for certain rheological combinations the central

"plug" in the spacer upstream will be moving slower than the central plug in the mud flow downstream. In this situation, the mud appears to be "pulling" the spacer down the center of the channel. The condition for this to happen is that:

$$B_s > B_m, \quad (6)$$

where B_m is the Bingham number of the mud, defined by:

$$B_m = \frac{D \times YP_m}{U_0 \times PV_m}. \quad (7)$$

Suppose Equation 6 holds. If now we consider the velocity profile upstream, for an increasingly thick static layer of mud, it is clear that, as the static layer grows thicker, the velocity of the plug region in the spacer will increase, since the total flow rate remains constant. Eventually, the plug in the spacer upstream will move faster than the plug in the mud downstream, and the spacer will again "push" the mud. In Ref. 29 it was shown that when the spacer pushes the mud in the center of the channel it is possible to find a velocity field that satisfies the steady problem, for a range of different fixed interfaces. In other words, when Equation 6 holds, there will be a minimum layer thickness, say Dh_{\min} , such that only uniform mud layers thicker than Dh_{\min} can be both static and allow a steadily propagating displacement. Figure 6 shows the variation in h_{\min} for different values of B_m and B_s .

Limiting Layers for Recirculation

A third limiting layer thickness can be derived that is of interest, (Ref. 28). Consider the steadily propagating finger displacement in Fig. 3. When viewed in the moving frame of reference, the steady interface corresponds to a streamline for the flow. The spacer fluid is always recirculating internally to the finger (as shown schematically in Fig. 7). If the static mud layers are sufficiently thick, the streamlines in the mud regions will flow smoothly around the finger, (Fig. 7a). On the other hand, as the static mud layer becomes thinner, there will always be a critical thickness below which the mud streamlines begin to recirculate upstream of the finger, (Fig. 7b). In fact this thickness is simple to compute; it is the thickness where the "plug" velocity in the mud is equal to the steady finger propagation speed. This layer thickness, say Dh_{circ} , will depend only on the Bingham number of the mud, B_m , and Fig. 8 shows the variation in h_{circ} with $1/B_m$.

Example Analytical Results

To illustrate the variation of the analytical results with different rheological parameters, we consider a slot of width $2D = 0.02$ m, containing mud of density 1600 kgm^{-3} , yield stress $YP_m = 18$ Pa, and plastic viscosity $PV_m = 120$ cP. We displace the mud with a spacer having the same density, yield point $YP_s = 7.2$ Pa, and plastic viscosity $PV_s = 24$ cP, using a mean displacement velocity $U_0 = 0.15 \text{ ms}^{-1}$. Taking these parameters as a base case, we vary each of the rheological parameters in turn and also the mean velocity. The results are shown in Figs. 9a and 9b for variations in the yield stresses,

and in Figs 10a and 10b for variations in the plastic viscosities.

It can be seen that h_{\max} decreases with YP_s , increases with YP_m , decreases with PV_s and is independent of PV_m . In contrast, h_{circ} is independent of YP_s , decreases with YP_m , is independent of PV_s and increases with PV_m . The layer thickness h_{\min} increases with YP_s , decreases with YP_m , decreases with PV_s and increases with PV_m .

Comparisons with CFD results

In the absence of displacement experiments, for a slot geometry, the CFD simulations represent the closest to reality that we are able to achieve. From this perspective it is of great interest to compare results from the CFD simulations with the different layer thicknesses h_{\max} , h_{\min} and h_{circ} . We have taken the base process parameters of the previous section and run a large number of CFD simulations. For each simulation, we measure the average layer thickness left after displacing one volume of fluid through the slot. In Fig. 11 we show this comparison, for the layer thicknesses computed in Fig. 9. Similarly, in Fig. 12 we make this comparison with the layer thicknesses computed in Fig. 10. After pumping one displacement volume, certain of the residual layers (i.e. the mud) are fully static, whilst others continue to move. The fully static layers are marked in Figs. 11 and 12 with a cross and the mobile layers are marked with a circle.

Two points are evident in Figs. 11 and 12. First, fully static layers are only found when the computed layers are less than the corresponding value of h_{\max} . Second, the fully static layer thicknesses are predicted remarkably well by the computed values of $h_{\text{circ}} < h_{\max}$. By extending the computations of mobile layers, we found that some of these would eventually decrease to thicknesses less than h_{\max} and stabilize. Other mobile layers appeared to decrease slowly to zero. We were unable to differentiate between parameters for which residual mud remained at long times. However, stable static mud layers were found only in the regime $h_{\text{circ}} < h_{\max}$.

The results in Figs. 11 and 12 are still more remarkable since they appear to follow well the variations in prediction h_{circ} with each parameter, e.g. see Fig. 11b. The prediction of h_{circ} , as an indicator of mud layer thickness, is obviously good, but is also quite counter-intuitive. For example, increasing the spacer yield stress or plastic velocity (Figs. 11a,12a) does not appear to affect the static layer thickness, until the layer is no longer static. When we actually have a static layer, increasing the mud yield stress appears to decrease the remaining layer thickness, (see Fig. 11b), but note that if the mud yield stress is small enough, no static layer will exist. These results cannot be predicted by a rudimentary analysis. It is clear that we need to distinguish clearly between situations where a static mud wall layer can and cannot exist, since if a static mud layer exists, our intuitive notions of how to treat it may be entirely wrong!

Effect of increasing velocity

A further unexpected effect happens on increasing the mean velocity of the displacement. In Fig. 13 we show the effect of varying U_0 for our base case in Figs. 9 and 10. Again the comparison with the CFD results is good. We see that, provided that a static layer can exist, the thickness predicted by $h_{\text{circ}} < h_{\max}$ actually increases with U_0 ! Eventually, we have that $h_{\text{circ}} > h_{\max}$ and the layers are no longer static. This shows that the conventional oilfield wisdom of pumping faster may not always improve the displacement.

Results in a Pipe

Our results for a pipe displacement are less complete than the slot displacement. There are three reasons for this. First, we are unable to design suitable laboratory fluids with arbitrary yield stresses and viscosities. In fact only a limited range rheologies have been possible with Carbopol solutions and although other fluids are available, they do not have the same degree of inelasticity as Carbopol and/or they are not suitable for visualization. Second, in displacing any particular Carbopol solution, we found that our range of flow rates was limited both above and below. If the flow rates were too low, the gelled Carbopol tends to fracture and if too high, then the Carbopol would slip at the pipe wall. Both of these affects are not representative of the wellbore situation, nor are they compatible with the models that we have used. Figure 14 shows an example of a Carbopol displacement at a flow rate for which fluid-like behavior is exhibited. It can be seen that the static residual layer is quite uniform. A third problem comes with the CFD simulations. Although the CFD computations perform well when the rheologies of the two fluids are comparable, when large rheology differences were simulated the CFD simulations deteriorated rapidly and were deemed unreliable. This is the case for all of the experimental series that have been run.

To demonstrate that the analytical results do predict well CFD-computed layer thicknesses in a pipe, we have performed a series of simulations for which the viscosities of the two fluids are comparable. The analytical results derived are easily generalized to the pipe geometry and to the Herschel-Bulkley rheologies that are characteristic of Carbopol solutions. For our test computations we assume a tube of diameter $D = 0.24$ m, fluid densities 1000 kgm^{-3} , $YP_s = 2$ Pa and $PV_s = 120$ cP. The mud we assume to be Herschel-Bulkley, with $YP_m = 5$, $PV_m = 1200$ cP, and index $n = 1$ as our default set of parameters. Figures 15, 16 and 17 show the comparison between the computed values of layer thickness and the values of h_{circ} , both expressed as a percentage of the tube radius. In these three figures we have varied the mud yield stress, the plastic viscosity (consistency) and the power law index, respectively, while keeping all other parameters fixed. It is evident that the predictive validity of h_{circ} is as good for the tube as for the slot. Qualitatively, the variations with mud yield stress and plastic viscosity are analogous to the same variations in a slot. The effect of shear thinning on the mud appears to be to thin the static layers. We also comment that

the static layers are comparatively thicker in the tube, than in the slot.

Having established the validity of our analytical model for the tube, in similar rheological conditions as for the slot, we now make comparisons the layer thickness h_{circ} predicted by the recirculation theory for a Herschel-Bulkley fluid in a pipe and the experimental layer thickness measured. Five different fluids have been tested, with properties as in Table 1. We have displaced different combinations of these fluids, in four series of experiments. The displaced and displacing fluids in each series are listed in Table 2. In each series of experiments, we have displaced the same fluids at a range of different flow rates. Figs. 18-21 show the results of each experimental series, comparing the prediction h_{circ} with the experimental layer thickness. It can be seen that in each case the prediction is good.

Interpretation

It would appear that for both numerical and experimental results, the value h_{circ} provides a good prediction of the static layer thickness. We present this here as an empirical fact.

In Ref. 28, we have attempted to provide a physical explanation for this remarkable prediction. The explanation centers on the supposition that the fluid rheologies are approximately equal. In this case, reducing the static layer thickness can be argued to reduce the local visco-plastic energy dissipation rate, at least until recirculation starts in the displaced fluid (the mud). Since the mud rheology will be higher than the displacing fluid rheology in the case of a static layer, if the mud is forced to recirculate, the local visco-plastic energy dissipation rate is likely to increase. This means that somewhere close to the recirculation layer thickness, h_{circ} , there is likely to be a local minimum in the visco-plastic energy dissipation rate. We believe that it is this layer thickness that is selected during the displacement.

This argument appears to be reasonable for comparable rheologies, (in cementing displacements, the fluid rheologies do compete with each other), but it would not hold for limiting rheological cases, e.g. where a gas bubble migrates through a drilling mud. For such limits we would need a separate analysis. For laminar cementing displacements, the rheologies are typically comparable. It appears that when $h_{max} > h_{circ}$, there can be a static layer on the wall and h_{circ} provides a reasonable prediction of the layer thickness.

The criterion $h_{max} = 0$ is the erodability criteria of Ref. 23. This criterion is often difficult to assure for all displacements. The only condition under which we have always had a static layer is $h_{max} > h_{circ}$. Therefore, it appears that the condition $h_{max} = 0$ (the erodability criterion) is not necessary for a displacement not to leave behind a static wall layer, although it is a sufficient condition. In many cases, the criterion $0 < h_{max} < h_{circ}$ is a sensible secondary goal and will ensure effective displacement.

The analysis we have carried out here can be combined with predictions from a two-dimensional simulation of eccentric annular displacements, (e.g. Ref. 19). Doing this gives a method to predict locally, at each point in a cemented annulus, whether or not a mud layer remains on the walls of the annulus, i.e. predicting the occurrence of a fluid-filled micro-annulus.

Conclusions and Further Work

We have presented results from detailed experimental mathematical and numerical analyses of displacements of visco-plastic fluids (muds) in long ducts. We have focused specifically on the case where a static residual layer of mud can remain on the walls of the duct. We have shown that we are able to predict when this occurs and approximate the layer thickness that remains, as a function of the rheological and other process parameters. It is these predictions that give rheological targets for applied chemistry solutions.

The above results hold for iso-density displacements. Although for horizontal wells, density differences are likely to be detrimental to displacement efficiency, density differences are the norm in primary cementing displacements. As soon as density differences are included in the analysis, it becomes necessary to include slot inclination. This significantly complicates the problem considered and forms the subject of ongoing research.

Acknowledgements

We thank the management of Schlumberger for their permission to publish this paper.

References

1. R.H. McLean, C.W. Manry and W.W. Whitaker, Displacement Mechanics in Primary Cementing. Society of Petroleum Engineers paper number SPE 1488, (1966).
2. A. Jamot, Deplacement de la boue par le latier de ciment dans l'espace annulaire tubage-paroi d'un puits. Revue Assoc. Franc. Techn. Petr., **224**, pp. 27-37, (1974).
3. C.F. Lockyear and A.P. Hibbert, *Integrated Primary Cementing Study Defines Key Factors for Field Success*. Journal of Petroleum Technology, December 1989, pp. 1320-1325.
4. C.F. Lockyear, D.F. Ryan and M.M. Gunningham, *Cement Channelling: How to Predict and Prevent*. Society of Petroleum Engineers paper number SPE 19865, (1989).
5. D. Guillot, H. Hendriks, F. Callet and B. Vidick, *Mud Removal*. Chapter 5 in *Well Cementing*. editor E.B. Nelson, Schlumberger Educational Services, Houston, (1990).
6. M. Couturier, D. Guillot, H. Hendriks and F. Callet, *Design Rules and Associated Spacer Properties for Optimal Mud Removal in Eccentric Annuli*. Society of Petroleum Engineers, paper number SPE 21594, (1990).
7. S. Brady, P.P. Drecq, K.C. Baker and D.J. Guillot, *Recent Technological Advances Help Solve Cement Placement Problems in the Gulf of Mexico*. Society of Petroleum Engineers paper IADC/SPE 23927, (1992).
8. D.F. Ryan, D.S. Kellingray and C.F. Lockyear, *Improved Cement Placement on North Sea Wells Using a Cement Placement Simulator*. Society of Petroleum Engineers paper number SPE 24977, (1992).

9. V.C. Kelessidis, R. Rafferty, A. Merlo and R. Maglione, *Simulator Models U-tubing to improve primary cementing*. Oil and Gas Journal, March 7th 1994, pp. 72-80.
10. S.R. Keller, R.J. Crook, R.C. Haut and D.S. Kulakofsky, *Deviated-Wellbore Cementing: Part 1 - Problems*. Journal of Petroleum Technology, August 1987, pp. 955-960.
11. R.J. Crook, S.R. Keller, and M.A. Wilson, *Deviated Wellbore Cementing: Part 2 - Solutions*. Journal of Petroleum Technology, August 1987, pp. 961-966.
12. F.L. Sabins, *Problems in Cementing Horizontal Wells*. Journal of Petroleum Technology, April 1990, pp. 398-400.
13. I.C. Walton and S.H. Bittleston, *The axial flow of a Bingham Plastic in a narrow eccentric annulus*, J. Fluid Mech., **222**, pp. 39-60, (1991).
14. P. Szabo and O. Hassager, *Flow of viscoplastic fluids in eccentric annular geometries*. J. Non-Newtonian Fluid Mech., **45**, pp. 149-169, (1992).
15. P. Szabo and O. Hassager, *Simulation of Free Surfaces in 3-D with the Arbitrary Lagrange-Euler Method*. Int. J. Num Methods in Eng., **38**, pp. 717-734, (1995).
16. P. Szabo and O. Hassager, *Displacement of One Newtonian Fluid by Another: Density Effects in Axial Annular Flow*. Int. J. Multiphase Flow, **23**(1), pp. 113-129, (1997).
17. M. Martin, M. Latil and P. Vetter, *Mud Displacement by Slurry during Primary Cementing Jobs - Predicting Optimum Conditions*. Society of Petroleum Engineers paper number SPE 7590, (1978).
18. A. Tehrani, S.H. Bittleston and P.J.G. Long, *Flow instabilities during annular displacement of one non-Newtonian fluid by another*. Experiments in Fluids 14, pp. 246-256, (1993).
19. A. Tehrani, J. Ferguson and S.H. Bittleston, *Laminar Displacement in Annuli: A Combined Experimental and Theoretical Study*. Society of Petroleum Engineers paper number SPE 24569, (1992).
20. R.W. Flummerfelt, *An Analytical Study of Laminar Non-Newtonian Displacement*. Society of Petroleum Engineers paper number SPE 4486, (1973).
21. R.M. Beirute and R.W. Flummerfelt, *Mechanics of the Displacement Process of Drilling Muds by Cement Slurries using an Accurate Rheological Model*. Society of Petroleum Engineers paper number SPE 6801, (1977).
22. A.N. Alexandrou and V. Entov, *On the steady-state advancement of fingers and bubbles in a Hele-Shaw cell filled by a non-Newtonian fluid*. Euro. Jnl. Of Applied Mathematics, **8**, pp. 73-87, (1997).
23. K.M Ravi, R.M. Beirute and R.L. Covington, *Erodability of Partially Dehydrated Gelled Drilling Fluid and Filter Cake*. Society of Petroleum Engineers paper number SPE 24571, (1992).
24. E. Lajeunesse, J. Martin, N. Rakotomalala, N. and D. Salin, *3D Instability of miscible displacements in a Hele-Shaw cell*. Phys. Rev. Lett., **79**, pp. 5254-5257, (1997).
25. E. Lajeunesse, J. Martin, N. Rakotomalala D. Salin, and Y. Yortsos, *Miscible Displacement in a Hele Shaw Cell at High Rates*. J. Fluid Mech., **398**, pp. 299-319 (1999).
26. P.G. Saffman and G.I. Taylor, *The penetration of a finger into a porous medium in a Hele-Shaw cell containing a more viscous liquid*. Proc. Roy. Soc. Lond. A **245**, pp. 312, (1958).
27. C. Gabard, *Etude de la stabilité de films liquides sur les parois d'une conduite verticale lors de l'écoulement de fluides miscibles non-newtoniens*. These de l'Universite Pierre et Marie Curie (PhD thesis), Orsay, France, in preparation, 2000.
28. M. Allouche, I.A. Frigaard, and G. Sona, *Static wall layers in the displacement of two visco-plastic fluids in a plane channel*. J. Fluid Mech., **424**, pp. 243 - 277 (2000)
29. I.A. Frigaard, O. Scherzer and G.Sona, *Uniqueness and non-uniqueness in the steady displacement of two viscoplastic fluids*. Submitted to ZAMM, November 1999, accepted for publication, to appear.

#	Description of fluid	YP (Pa)	K (Pa·s ⁿ)	n
1	1.4g Carbopol in glycerol	2.5	25.7	0.467
2	1.5g Carbopol in glycerol	5.0	32.08	0.464
3	Water	0.0	0.0018	1.0
4	0.7g Carbopol in sucrose	0.0	0.18	0.745
5	1.4g Carbopol in sucrose	1.0	6.77	0.48

Table 1: - Rheology of fluids used in displacement experiments

Experimental Series	Displaced Fluid	Displacing Fluid
Series 1	Fluid 1	Fluid 3
Series 2	Fluid 2	Fluid 3
Series 3	Fluid 2	Fluid 4
Series 4	Fluid 2	Fluid 5

Table 2: - Description of fluids used in each experimental series

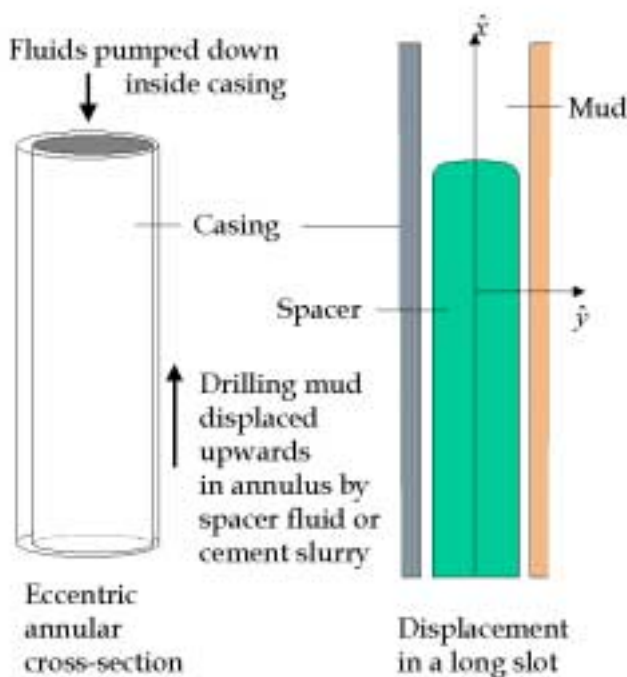


Fig. 1 - Schematic of a cementing displacement, focusing on what happens in an axial cross-section of the annular gap, i.e. a slot.

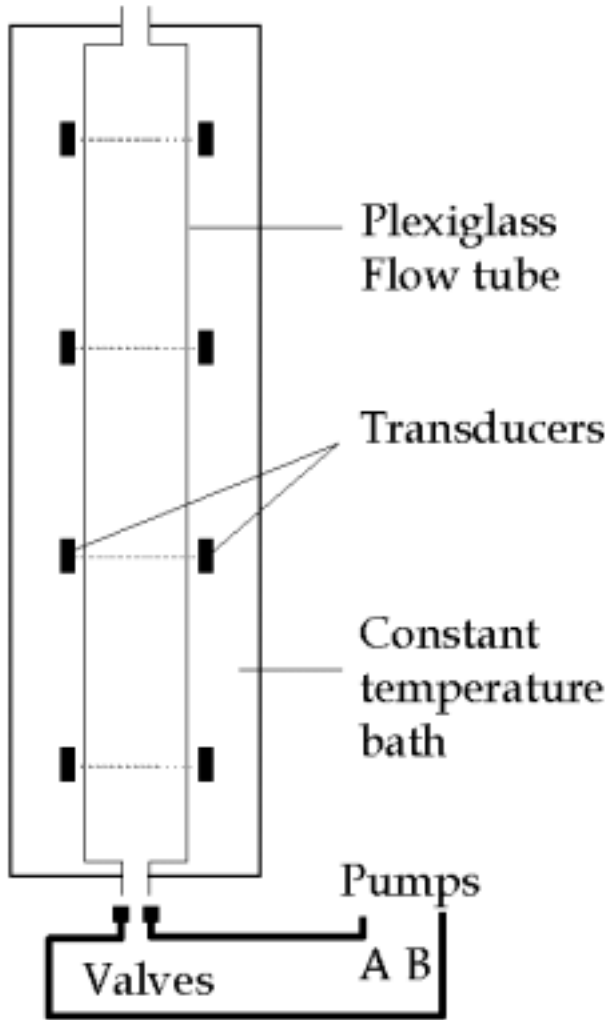


Fig. 2 - Schematic of the experimental setup.

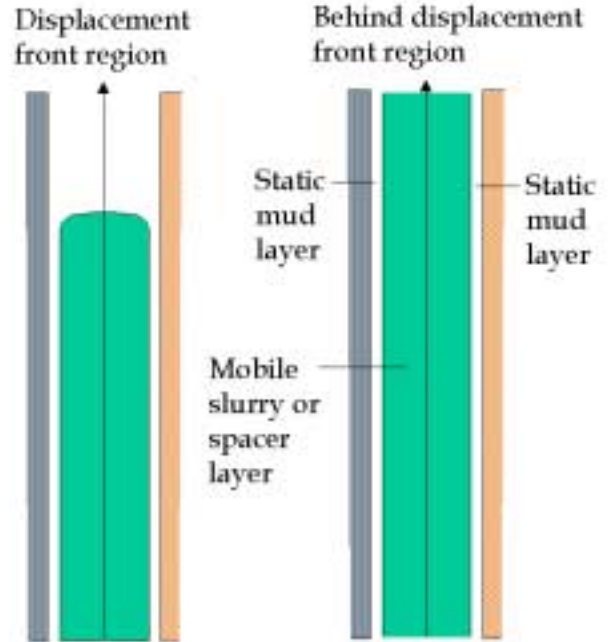


Fig. 3 - Parallel multi-layer flow allowing static mud layers on the walls, existing far behind the displacement front.

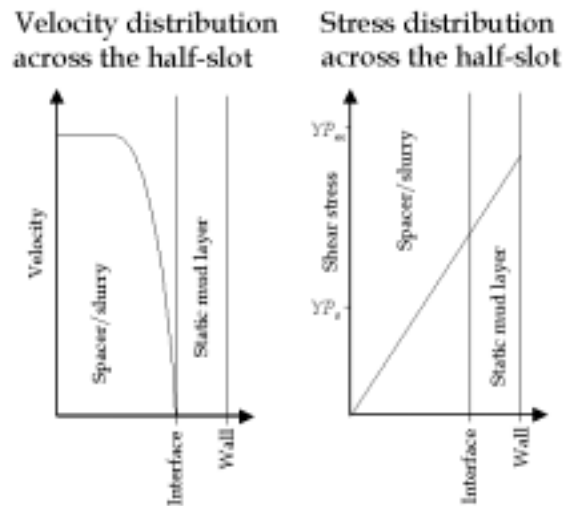


Fig. 4 - Schematic of velocity and stress profiles that admit a static mud wall layer.

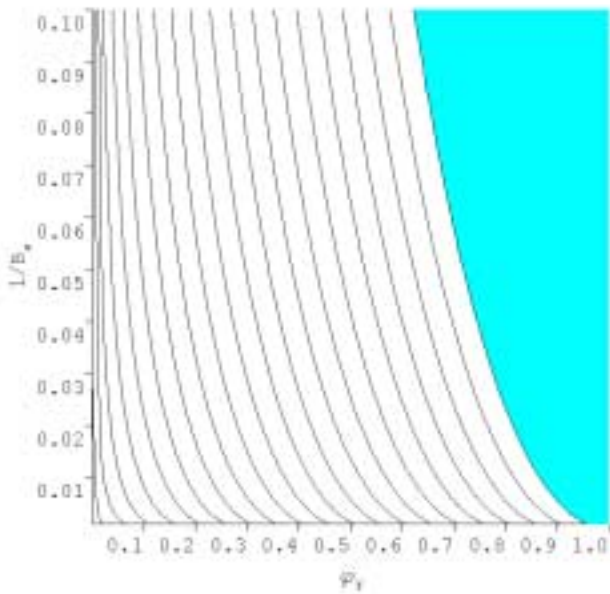


Fig. 5 - Contours of h_{max} plotted against spacer/slurry Bingham number and yield stress ratio. In the shaded area $h_{max} = 0$, and outside of this area, contours represent 5% of the slot width.

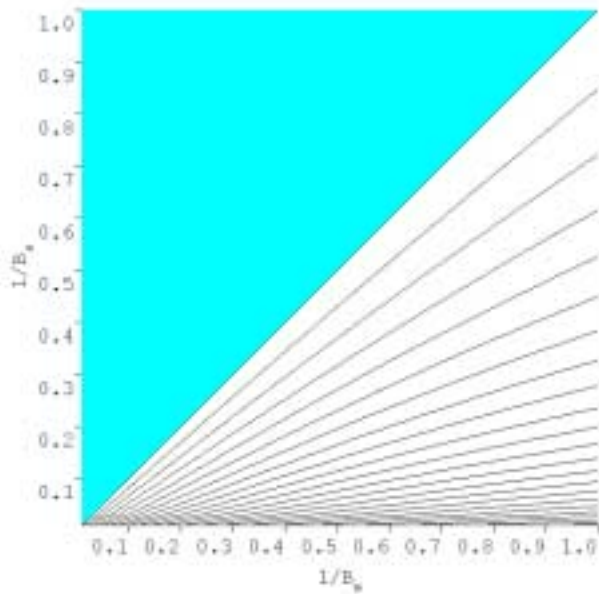


Fig. 6 - Contours of h_{min} plotted against spacer/slurry Bingham number and mud Bingham number. In the shaded area $h_{min} = 0$, and outside of this area, each contour represents 1% of the slot width.

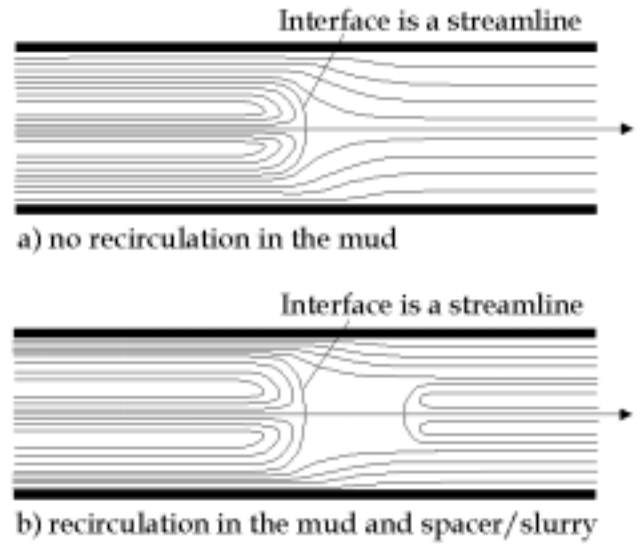


Fig. 7 - Schematic behaviour of fluid streamlines as viewed in a moving frame of reference, moving with the same velocity as the steadily propagating finger displacement. a) The mud streamlines flow smoothly around the interface for thick enough static wall layers. b) The mud streamlines contain recirculatory zones and do not all flow around the interface, for a thin enough static layer.

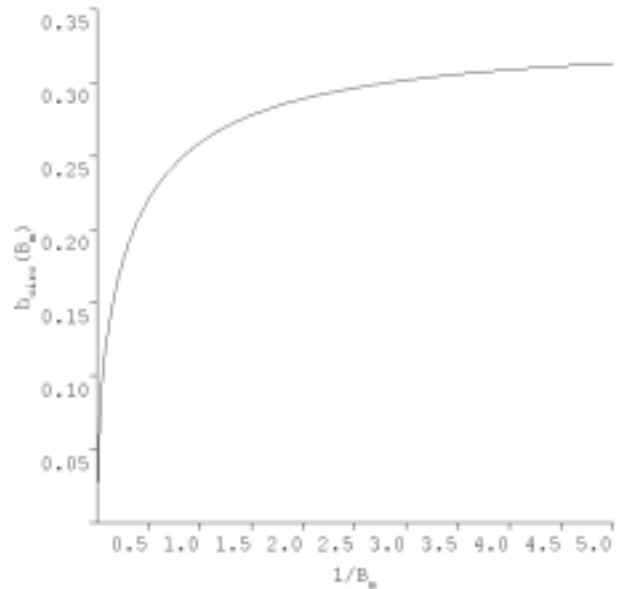


Fig. 8 - Variation in h_{circ} , plotted against $1/B_m$.

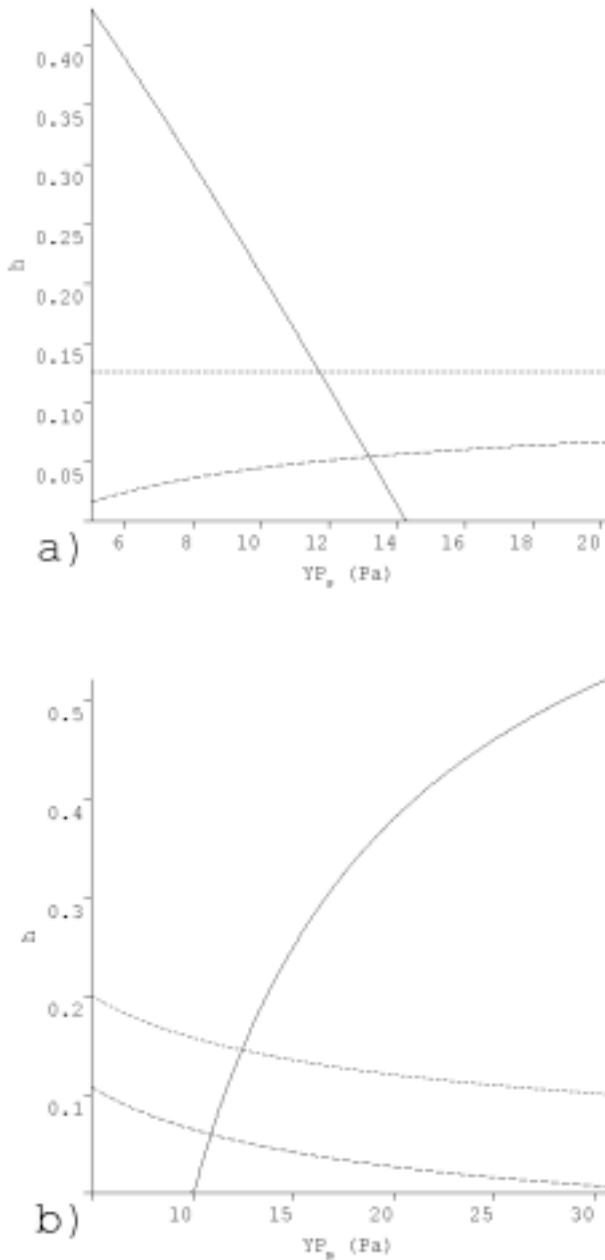


Fig. 9 - Variations in h_{\max} (solid line), h_{circ} (uppermost dashed line), and h_{\min} (lower dashed line), for a base case of: slot half-width $D = 0.01$ m, fluid densities 1600 kgm^{-3} , mud yield stress $YP_m = 18$ Pa, mud plastic viscosity $PV_m = 120$ cP, spacer yield point $YP_s = 7.2$ Pa, spacer plastic viscosity $PV_s = 24$ cP, mean displacement velocity $U_0 = 0.15 \text{ ms}^{-1}$. a) Variations with YP_s . b) Variations with YP_m .

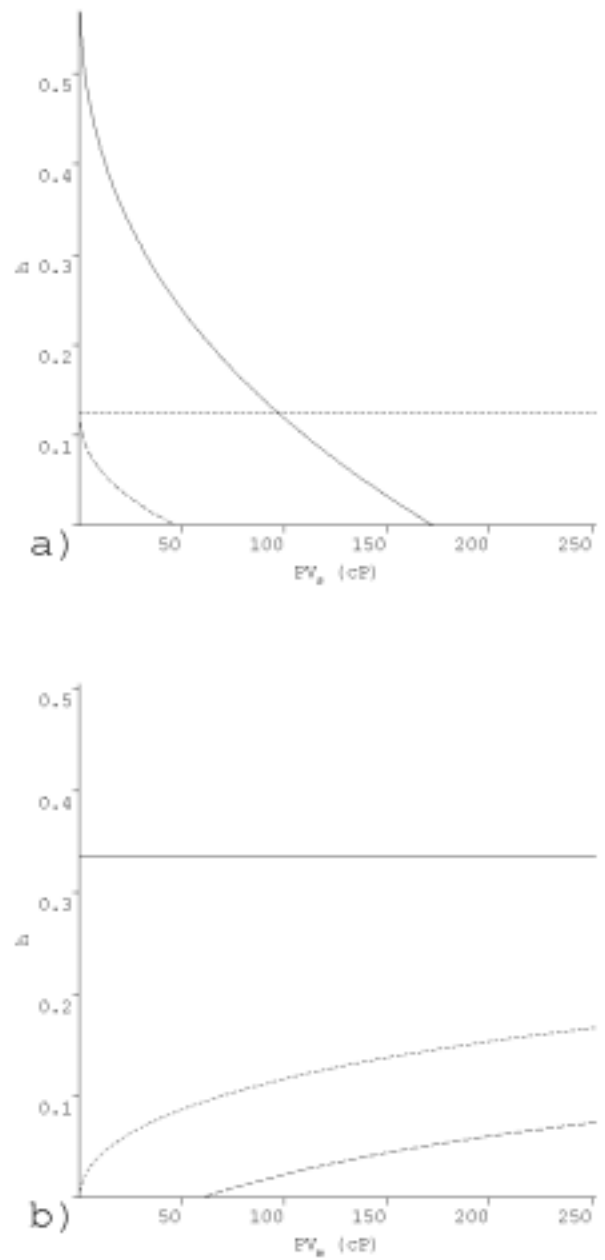


Fig. 10 - Variations in h_{\max} (solid line), h_{circ} (uppermost dashed line), and h_{\min} (lower dashed line), for a base case of: slot half-width $D = 0.01$ m, fluid densities 1600 kgm^{-3} , mud yield stress $YP_m = 18$ Pa, mud plastic viscosity $PV_m = 120$ cP, spacer yield point $YP_s = 7.2$ Pa, spacer plastic viscosity $PV_s = 24$ cP, mean displacement velocity $U_0 = 0.15 \text{ ms}^{-1}$. a) Variations with PV_s . b) Variations with PV_m .

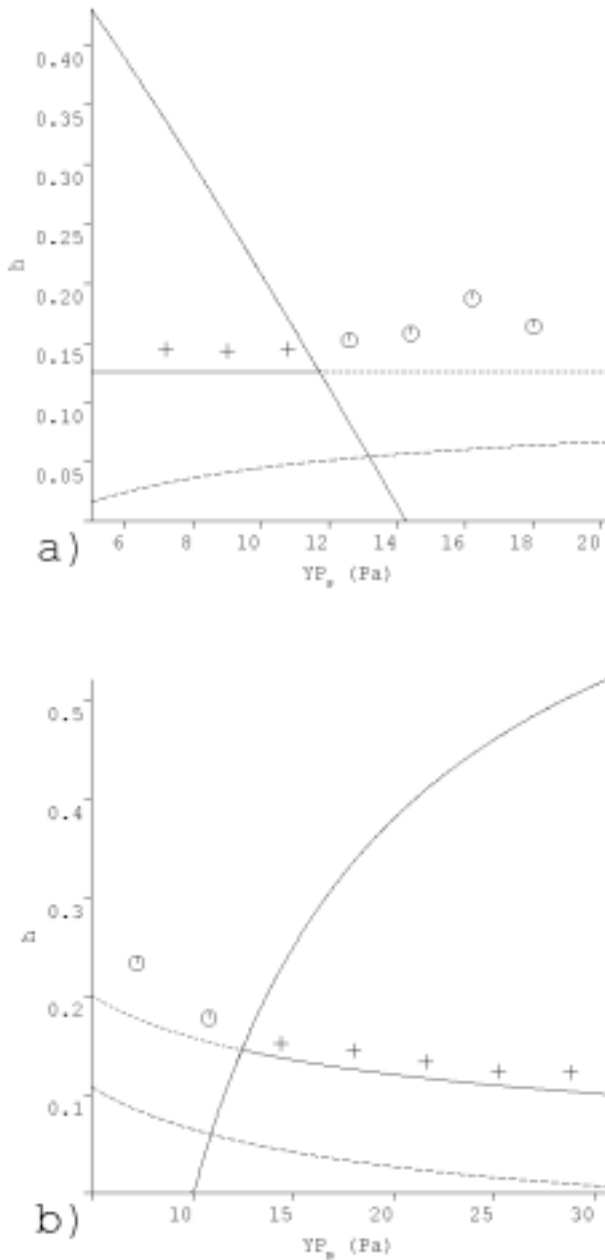


Fig. 11 - Comparisons of computed values of layer thickness from CFD computations with computed variations in h_{max} , h_{circ} and h_{min} , (compare with Fig. 9), for a base case of: slot half-width $D = 0.01$ m, fluid densities 1600 kgm^{-3} , mud yield stress $YP_m = 18$ Pa, mud plastic viscosity $PV_m = 120$ cP, spacer yield point $YP_s = 7.2$ Pa, spacer plastic viscosity $PV_s = 24$ cP, mean displacement velocity $U_0 = 0.15 \text{ ms}^{-1}$. a) Variations with YP_s . b) Variations with YP_m . Points marked with + denote fully static layers. Points marked with O denote mud layers that are still moving.

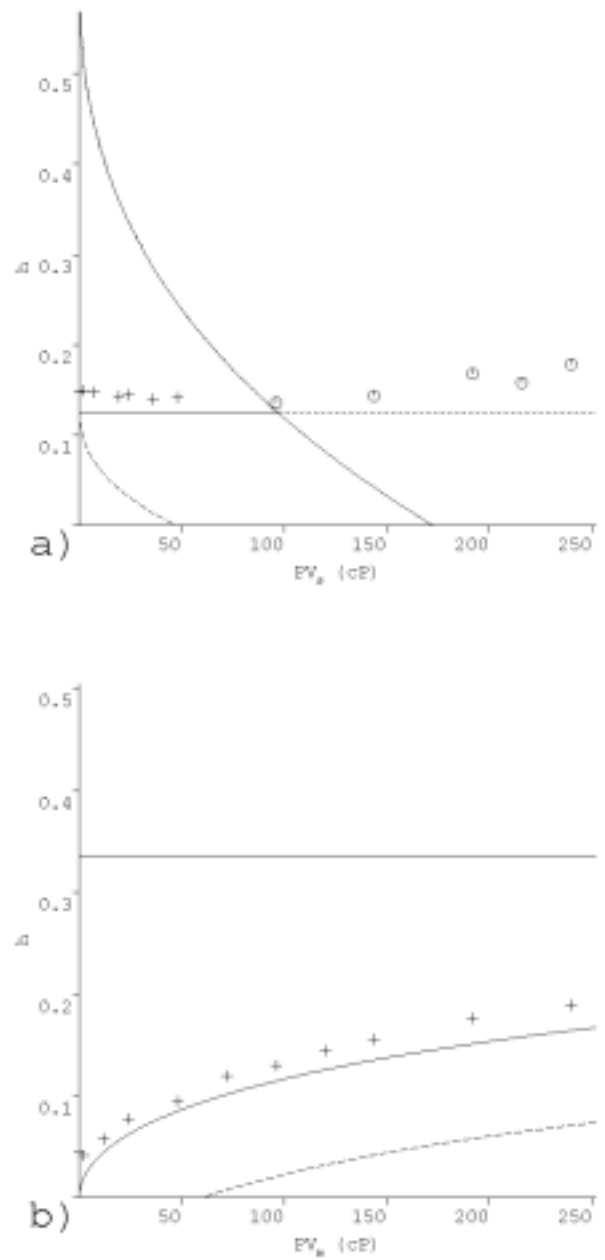


Fig. 12 - Comparisons of computed values of layer thickness from CFD computations with computed variations in h_{max} , h_{circ} and h_{min} , (compare with Fig. 10), for a base case of: slot half-width $D = 0.01$ m, fluid densities 1600 kgm^{-3} , mud yield stress $YP_m = 18$ Pa, mud plastic viscosity $PV_m = 120$ cP, spacer yield point $YP_s = 7.2$ Pa, spacer plastic viscosity $PV_s = 24$ cP, mean displacement velocity $U_0 = 0.15 \text{ ms}^{-1}$. a) Variations with PV_s . b) Variations with PV_m . Points marked with + denote fully static layers. Points marked with O denote mud layers that are still moving.

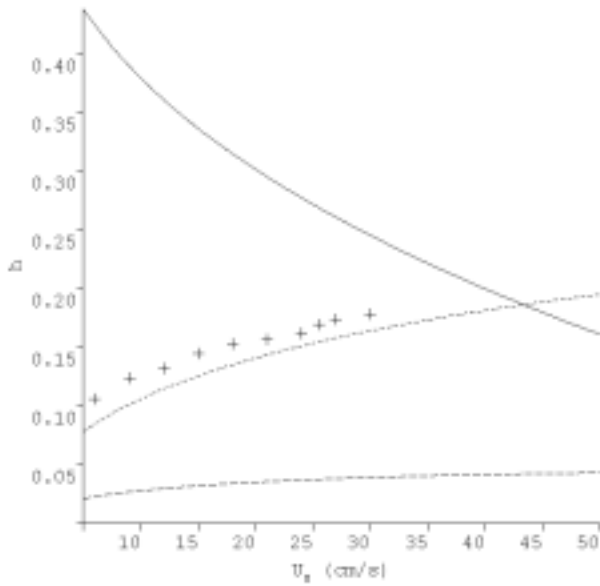


Fig. 13 - Comparisons of computed values of layer thickness from CFD computations with computed variations h_{max} (solid line), h_{circ} (uppermost dashed line), and h_{min} (lower dashed line). Variations against U_0 for a base case of: $D = 0.01$ m, fluid densities 1600 kgm^{-3} , $YP_m = 18$ Pa, $PV_m = 120$ cP, $YP_s = 7.2$ Pa, $PV_s = 24$ cP. Points marked with + denote fully static layers.

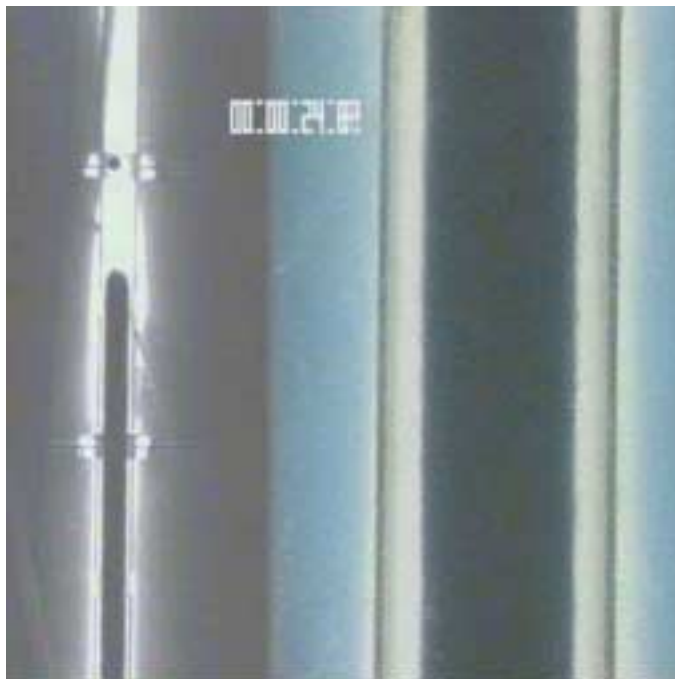


Fig. 14 - Example of a typical displacement of a Carbopol-glycerol solution by water. The left-hand side shows displacement front, clearly visible are the transducers (see Fig. 2). Right-hand side shows a close-up of the interface after the front has passed.

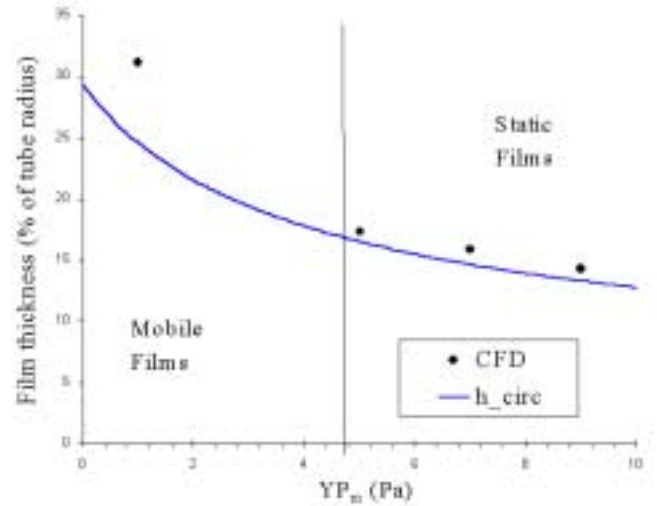


Fig. 15 - Comparisons of computed values of layer thickness from CFD computations with computed variations in h_{circ} . Variations against YP_m for displacements in a tube. Parameters are: diameter $D = 0.24$ m, fluid densities 1000 kgm^{-3} , $YP_s = 2$ Pa, $PV_m = 1200$ cP, $PV_s = 120$ cP. The vertical line marks the point at which h_{circ} exceeds h_{max} .

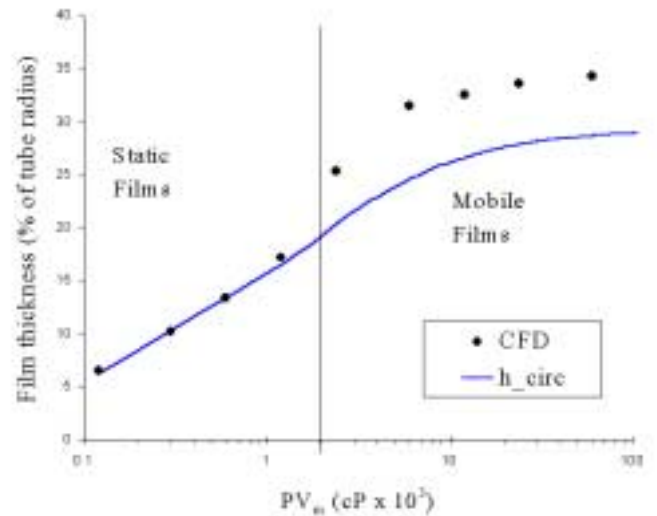


Fig. 16 - Comparisons of computed values of layer thickness from CFD computations with computed variations in h_{circ} . Variations against PV_m for displacements in a tube. Parameters are: diameter $D = 0.24$ m, fluid densities 1000 kgm^{-3} , $YP_m = 5$ Pa, $YP_s = 2$ Pa, $PV_s = 120$ cP. The vertical line marks the point at which h_{circ} exceeds h_{max} .

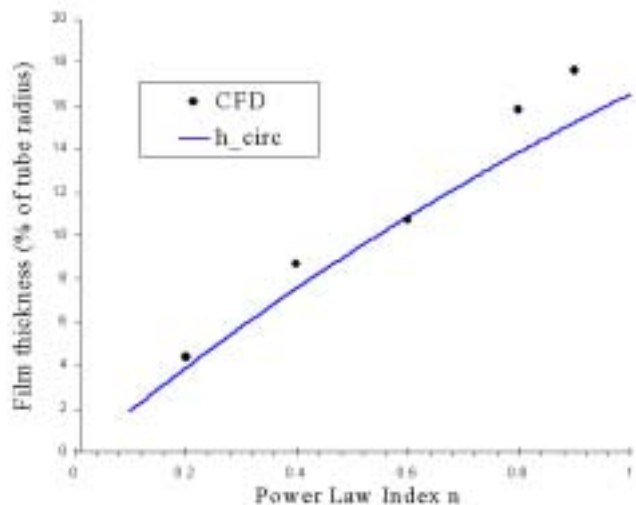


Fig. 17 - Comparisons of computed values of layer thickness from CFD computations with computed variations in h_{circ} . Variations against mud power law index n for displacements in a tube. Parameters are: diameter $D = 0.24$ m, fluid densities 1000 kgm^{-3} , $YP_m = 5 \text{ Pa}$, $YP_s = 2 \text{ Pa}$, $PV_m = 1200 \text{ cP}$, $PV_s = 120 \text{ cP}$.

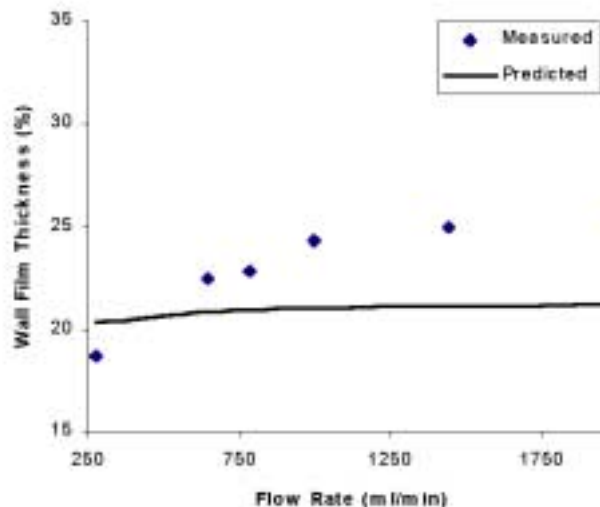


Fig. 19 - Comparison of predicted and measured layer thicknesses for experimental series 2: fluid 2 displaced by fluid 3.

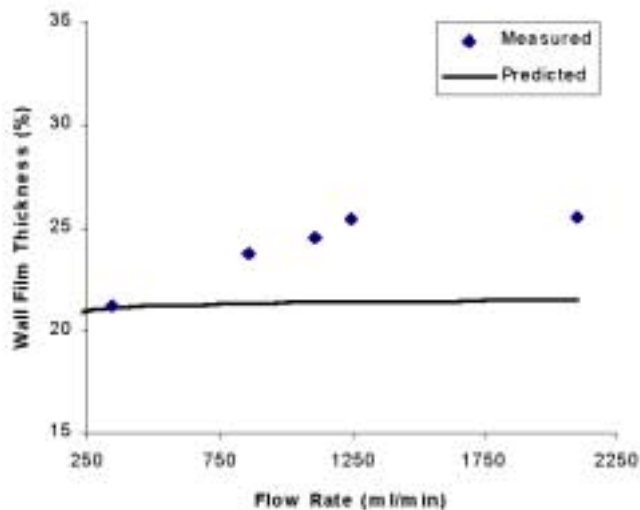


Fig. 18 - Comparison of predicted and measured layer thicknesses for experimental series 1: fluid 1 displaced by fluid 3.

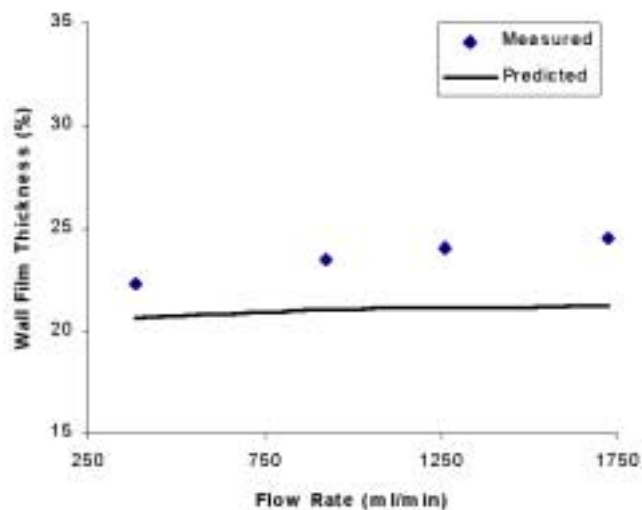


Fig. 20 - Comparison of predicted and measured layer thicknesses for experimental series 3: fluid 2 displaced by fluid 4.

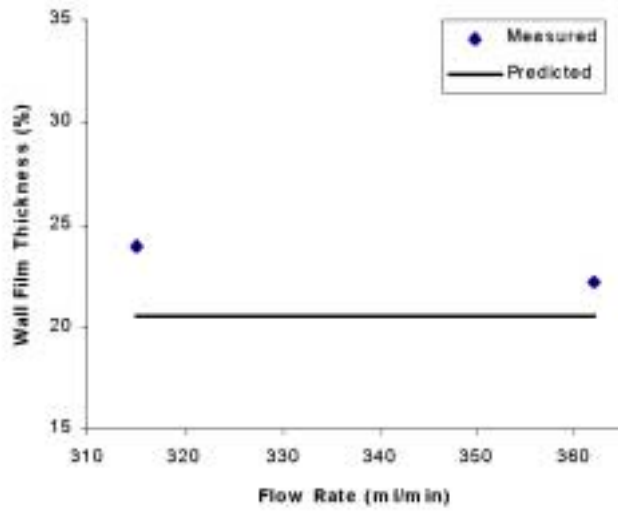


Fig. 21 - Comparison of predicted and measured layer thicknesses for experimental series 4: fluid 2 displaced by fluid 5.